Materials Chemistry and Physics 296 (2023) 127276

Contents lists available at ScienceDirect

Materials Chemistry and Physics

journal homepage: www.elsevier.com/locate/matchemphys

Perturbing the spin state and conduction of Fe (II) spin crossover complexes with TCNQ

Thilini K. Ekanayaka [a,*], Ökten Üngör [b], Yuchen Hu [c], Esha Mishra [a], Jared P. Phillips [d], Ashley S. Dale [d], Saeed Yazdani [d], Ping Wang [b], Kayleigh A. McElveen [c], M. Zaid Zaz [a], Jian Zhang [e], Alpha T. N'Diaye [f], Christoph Klewe [f], Padraic Shafer [f], Rebecca Y. Lai [c,g], Robert Streubel [a,g], Ruihua Cheng [d,**], Michael Shatruk [b,***], Peter A. Dowben [a,****]

[a] Department of Physics and Astronomy, University of Nebraska-Lincoln, Lincoln, NE, 68588-0299, USA
[b] Department of Chemistry and Biochemistry, Florida State University, 95 Chieftan Way, Tallahassee, FL, 32306, USA
[c] Department of Chemistry, University of Nebraska-Lincoln, Lincoln, NE, 68588-0299, USA
[d] Department of Physics, Indiana University-Purdue University Indianapolis, Indianapolis, IN, 46202, USA
[e] Molecular Foundry, Lawrence Berkeley National Laboratory, Berkeley, CA, 94720, USA
[f] Advanced Light Source, Lawrence Berkeley National Laboratory, Berkeley, CA, 94720, USA
[g] Nebraska Center for Materials and Nanoscience, University of Nebraska-Lincoln, North 16th Street, Lincoln, NE, 68588, USA

HIGHLIGHTS

- TCNQ anions may perturb the spin state of the spin crossover (SCO) molecules.
- The impedance of [Fe{$H_2B(pz)_2$}$_2$(bipy)] (Fe(II) SCO) molecular spin crossover systems is reduced by adding TCNQ.
- Fe(II) SCO mixed with TCNQ shows enhanced transistor carrier mobility on ferroelectric polyvinylidene fluoride thin film.
- For Fe(II) SCO mixed with TCNQ, the majority charge carriers appear to be holes.
- Fe(II) SCO mixed with TCNQ has a small but measurable transistor carrier mobility.

ABSTRACT

We investigated modifications driven by 7,7,8,8-tetracyanoquinodimethane (TCNQ) to the spin state configuration of [Fe(3-bpp)$_2$](TCNQ)$_2$ co-crystal and both spin state and electric conductivity of [Fe{$H_2B(pz)_2$}$_2$(bipy)] and TCNQ mixtures. The Fe^{2+} site in the [Fe(3-bpp)$_2$](TCNQ)$_2$ co-crystal has a sizable orbital moment. During X-ray absorption measurements, the iron ion is partially excited to the high spin state and strong surface effects are indicated. Mixing TCNQ with the [Fe{$H_2B(pz)_2$}$_2$(bipy)] spin crossover complex leads to a molecular combination with increased conductivity and drift carrier lifetimes. [Fe{$H_2B(pz)_2$}$_2$(bipy)] thin films with TCNQ, grown using dimethylformamide (DMF), are to great extent locked mainly in the low spin (LS) state across a broad temperature range and exhibit drift carrier lifetimes approaching 0.5 s. When deposited onto a ferroelectric polyvinylidenefluoride-hexafluoropropylene thin film substrate, [Fe{$H_2B(pz)_2$}$_2$(bipy)], shows enhanced transistor carrier mobility, likely associated with the increasing cationic character of [Fe{$H_2B(pz)_2$}$_2$(bipy)] thin films with TCNQ.

1. Introduction

While organic electronics has become increasingly attractive as a route to developing flexible nonvolatile memory devices [1–9], molecular spin crossover (SCO) materials with transition metal ions also show considerable promise for such devices [9,10]. Molecular SCO materials exhibit magnetic bistability due to a reversible transition between low spin (LS) and high spin (HS) states that can be triggered by external stimuli, such as pressure, temperature, magnetic field, light, and X-ray irradiation, or by adding guest molecules [11–15]. Critical for prospective applications is the realization of voltage-controlled isothermal spin state switching in SCO molecular films and a non-volatile

* Corresponding author.
** Corresponding author.
*** Corresponding author.
**** Corresponding author.
E-mail address: thiliniek@huskers.unl.edu (T.K. Ekanayaka).

https://doi.org/10.1016/j.matchemphys.2022.127276
Received 1 August 2022; Received in revised form 20 December 2022; Accepted 24 December 2022
Available online 28 December 2022

conductance change in heteromolecular structures with a molecular ferroelectric [16,17]. This conductance and spin state change introduces a facile "read" to a device based on molecular ferroelectric polarization reversal [10,16,17]. Although very convenient, there are complications with this voltage controlled read and write mechanism, i.e., a large on-state resistance that hinders a favourable comparison with the silicon technology [10]. Several molecular SCO systems with low resistivity have been reported [10,18]. The challenge is, though, to synthesize molecular SCO thin films with significantly lower impedance [10].

Combining polar molecules with SCO complexes is a way to achieve SCO materials with altered properties, particularly, affecting the temperature and abruptness of the spin state transition [19,20]. Adding polyaniline to the SCO complex $[Fe(Htrz)_2(trz)(BF_4)]$ was shown to result in a significant increase in the conductivity [21], with a strong dependence on the polyaniline concentration [21] and choice of polyaniline [22]. Aside from polyaniline, the organic acceptor molecule 7,7,8,8-tetracyanoquinodimethane (TCNQ) also shows promise for providing a route toward low-impedance SCO materials [18,23–30]. Due to its strong electron-acceptor character, TCNQ increases the cationic character of the SCO molecule [18,31] and lowers the resistance by providing conducting pathways in the hybrid material, especially when introduced as fractionally charged anions, i.e. $TCNQ^{\delta-}$ $(0 < \delta < 1)$ [18,23–28]. Several recent studies have reported co-crystallization of SCO cations with TCNQ anions [18,23,24,27], and the addition of TCNQ is frequently seen to affect the spin transition and conductivity in molecular materials.

Given the very limited number of studies investigating the change in charge carrier properties of potential device related SCO molecular thin films, we studied two different Fe(II) SCO complexes that include TCNQ as an additive: a $[Fe(3\text{-bpp})_2](TCNQ)_2$ co-crystal described previously [23,32] and a $[Fe\{H_2B(pz)_2\}_2(bipy)]$ complex in a matrix mixture with neutral TCNQ. The co-crystallization with TCNQ anions [23] makes the $[Fe(3\text{-bpp})_2](TCNQ)_2$ crystal highly conductive and opens a route to topologically protected currents in the transistor geometry, because of loss of inversion symmetry. The much investigated $[Fe\{H_2B(pz)_2\}_2(bipy)]$ SCO molecule has been used as a molecular transistor channel conductor in heteromolecular transistor structures that make effective nonvolatile memory devices [16,17], albeit with significant impedance [10]. Here, we show that adding TCNQ to a Fe(II) molecular SCO system reduces the impedance despite locking $[Fe\{H_2B(pz)_2\}_2(bipy)]$ in the LS state. The majority charge carriers appear to be holes, yielding a p-channel transistor.

2. Experimental

$[Fe(3\text{-bpp})_2](TCNQ)_2$ [23] (Fig. 1a) and $[Fe\{H_2B(pz)_2\}_2(bipy)]$ [33] were synthesized as discussed in the literature. The synthesis of $[Fe(qsal)_2][TCNQ_2]$ was adapted from two similar molecules [29,30] using a Li(TCNQ) precursor [34,35] and $[Fe(qsal)_2]Cl$ [36]. The Li(TCNQ) precursor was fabricated according to [34,35] where TCNQ, in anhydrous acetonitrile, was brought to a boil and then added to a boiling solution lithium iodide acetonitrile. The synthesis of $[Fe(qsal)_2]Cl$ was from 8-aminoquinoline and salicylaldehyde in methanol followed by the addition of $FeCl_3$ and triethylamine, as in [36]. The $[Fe(qsal)_2]Cl$ and Li(TCNQ) were then combined acetonitrile to form the $[Fe(qsal)_2][TCNQ_2]$. The $[Fe(qsal)_2][TCNQ_2]$ studies were done to confirm the influence of PVDF as a substrate on an Fe(III) complex with TCNQ. More of the characterization of $[Fe(qsal)_2][TCNQ_2]$ will be reported in future studies. $[Fe\{H_2B(pz)_2\}_2(bipy)]$ and TCNQ were mixed in a 1:1 ratio and dissolved in DMF prior to drop-casting. Both TCNQ and DMF were purchased from Sigma Aldrich. The organic field-effect transistor (OFET) chips were acquired from the Fraunhofer Institute for Photonics. The spacing of these interdigitated electrodes is 2.5 μm and the thickness of the dielectric layer is about 230 nm.

X-ray absorption spectroscopy (XAS) was done at the Advanced Light Source (ALS, beamline 6.3.1) at Lawrence Berkeley National Laboratory (Berkeley, CA) using total electron yield and right-handed circularly polarized X-rays. X-ray magnetic circular dichroism (XMCD) spectroscopy was carried out at beamline 4.0.2 at the ALS also using the total electron yield. A magnetic field of 3.6 T/μ_0 was applied normal to the plane of the thin-film sample. Since this field is insufficient to align and saturate the magnetic moment, the measured values for the spin and orbital moments are a mere fraction of the actual Fe (II) moments. The measurements were performed in the temperature range of 130 K–250 K. At each temperature, samples were equilibrated for 10–15 min. The $[Fe\{H_2B(pz)_2\}_2(bipy)]$ with TCNQ solution was drop-cast on a HOPG

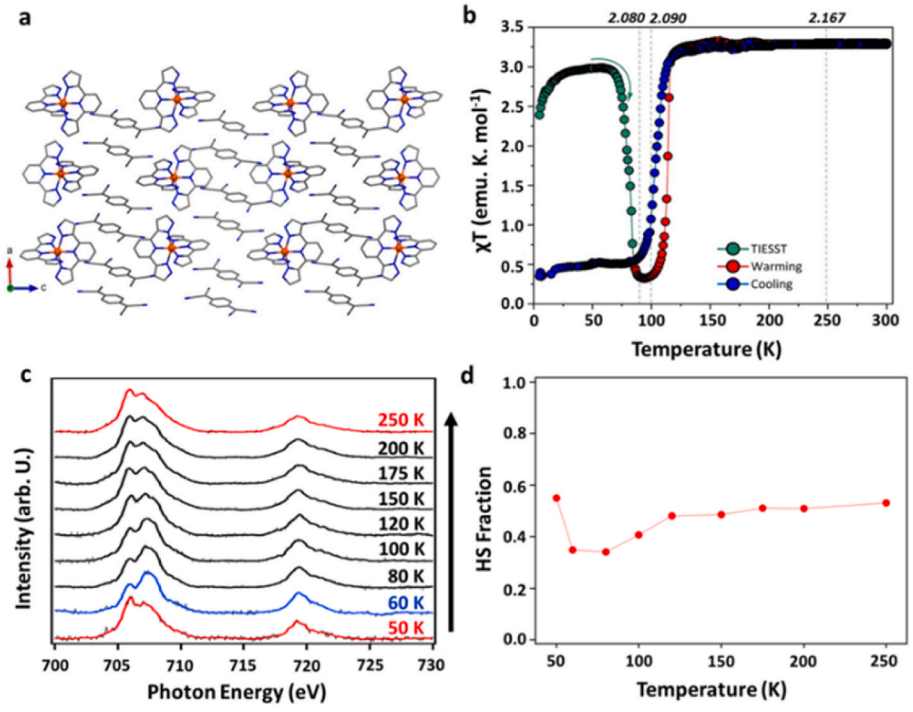

Fig. 1. (a) Crystal structure of $[Fe(3\text{-bpp})_2](TCNQ)_2$ (Fe = orange, N = blue and C = grey) and (b) temperature-dependent χT product of $[Fe(3\text{-bpp})_2](TCNQ)_2$ (the average Fe–N bond lengths at 90 K, 100 K, and 250 K are indicated by numbers in the top of the plot). (c) Temperature-dependent X-ray absorption spectra of $[Fe(3\text{-bpp})_2](TCNQ)_2$ (with the filtered data in bold). d) HS fraction extracted from c). (For interpretation of the references to colour in this figure legend, the reader is referred to the Web version of this article.)

substrate and the $[Fe(3\text{-}bpp)_2](TCNQ)_2$ co-crystal was crushed into powder and attached to a conducting carbon tape.

Thin films of $[Fe\{H_2B(pz)_2\}_2(bipy)]$ combined with TCNQ were fabricated on OFET chips with and without polyvinylidenefluoride-hexafluoropropylene (PVDF-HFP) film and prepared by drop-casting. About 10 nm thick film of PVDF-HFP was deposited onto the substrate using the Langmuir-Blodgett technique after established methods [37]. The PVDF-HFP pellets were obtained from Sigma Aldrich and dissolved in acetone to create a 0.05% by weight solution. This solution was then drop cast onto a subphase of ultrapure 18 MΩ water and the acetone was allowed to evaporate leaving behind a PVDF-HFP monolayer. The monolayer was transferred to the Fraunhofer substrate at a rate of 1.9 mm/s and allowed to dry completely between layers. Transport measurements were conducted using a 4200A-SCS parameter analyser and cryogenic Lakeshore probe station. We found the challenges of making a uniform molecular thin film, from solution, presently insurmountable as the $[Fe(3\text{-}bpp)_2](TCNQ)_2$ favors co-crystallization and does not form a thin film suitable for electrical transport measurements. Üngör et al. [23] reported electrical resistance measurements, however, from $[Fe(3\text{-}bpp)_2](TCNQ)_2$ single crystals using a four-point-probe method. A 2nd-order Savitzky-Golay (SG) filter was applied to the data to create Figs. 1c and 2a. A 7-point SG and 25-point SG were used for resonance and non-resonance regions respectively so that absorption features can be retained even with the smoothing. The filtered data are presented with unprocessed data.

3. Spin-crossover monitored by X-ray absorption spectroscopy

One benchmark for tracking the spin transition is the change in magnetic susceptibility (χ) as a function of the temperature (T) [11,13,23,25,28,32,33,38]. The magnetic susceptibility of $[Fe(3\text{-}bpp)_2](TCNQ)_2$ shows an abrupt spin transition with a thermal hysteresis of 9 K when using a heating and cooling rate of 2 K/min (Fig. 1b). This observation compares well with the temperature-induced SCO reported by Üngör et al. [23] who also showed that the HS state observed at higher temperatures can be trapped by flash cooling to 10 K.

The crystal structure of $[Fe(3\text{-}bpp)_2](TCNQ)_2$, determined from X-ray diffraction (XRD), reveals an average Fe–N bond lengths of 2.080 Å, 2.090 Å, and 2.167 Å at 90 K, 100 K, and 250 K, respectively [23]. The larger metal-to-ligand bond lengths in SCO complexes are associated with the conversion to the HS state [39], in agreement with the aforementioned magnetic behaviour of $[Fe(3\text{-}bpp)_2](TCNQ)_2$. However, while the magnetic data suggest a nearly complete LS state below 105 K, the Fe–N bond lengths observed at 90 K and 100 K indicate a considerable HS fraction under an X-ray fluence (the average Fe–N bond length expected for the LS state is 2.00 Å). The fraction of HS state occupancy, estimated as 40% at 90 K and 45% at 100 K, was hypothesized to stem from X-ray induced excited spin state trapping (XIESST) [11]. The material also shows a temperature-induced excited spin-state trapping (TIESST) effect at low temperatures, the first reported for any SCO complex combined with TCNQ [23]. The so-called TIESST state remains stable at low temperatures but decays rapidly to the ground LS state when the temperature exceeds 75 K. Further heating to 300 K and cooling to 5 K at 2 K/min follow the pathway of the hysteretic thermally induced spin transition observed upon initial cooling.

To confirm the presence of XIESST, we performed XAS on $[Fe(3\text{-}bpp)_2](TCNQ)_2$ co-crystals (Fig. 1c). The electronic transition from fully occupied Fe 2*p* orbitals to partially unoccupied 3*d* orbitals, measured by the *L*-edge XAS, indicates the weighted empty Fe 3*d* orbitals. Based on the ligand field theory, the 3*d* orbitals split in two energy states, t_{2g} and e_g [11–15]. Six Fe^{2+} 3*d* electrons occupy three t_{2g} orbitals in pairs in the LS state, resulting the two empty e_g orbitals. In the HS state, two electrons are promoted from t_{2g} to e_g, leaving both sets of orbitals partially occupied [11–15]. For $[Fe(3\text{-}bpp)_2](TCNQ)_2$, the excitations to the e_g and t_{2g} orbitals are observed at 708 eV and 706 eV, respectively, similar to the XAS transitions observed in other SCO systems [40–48]. The XAS

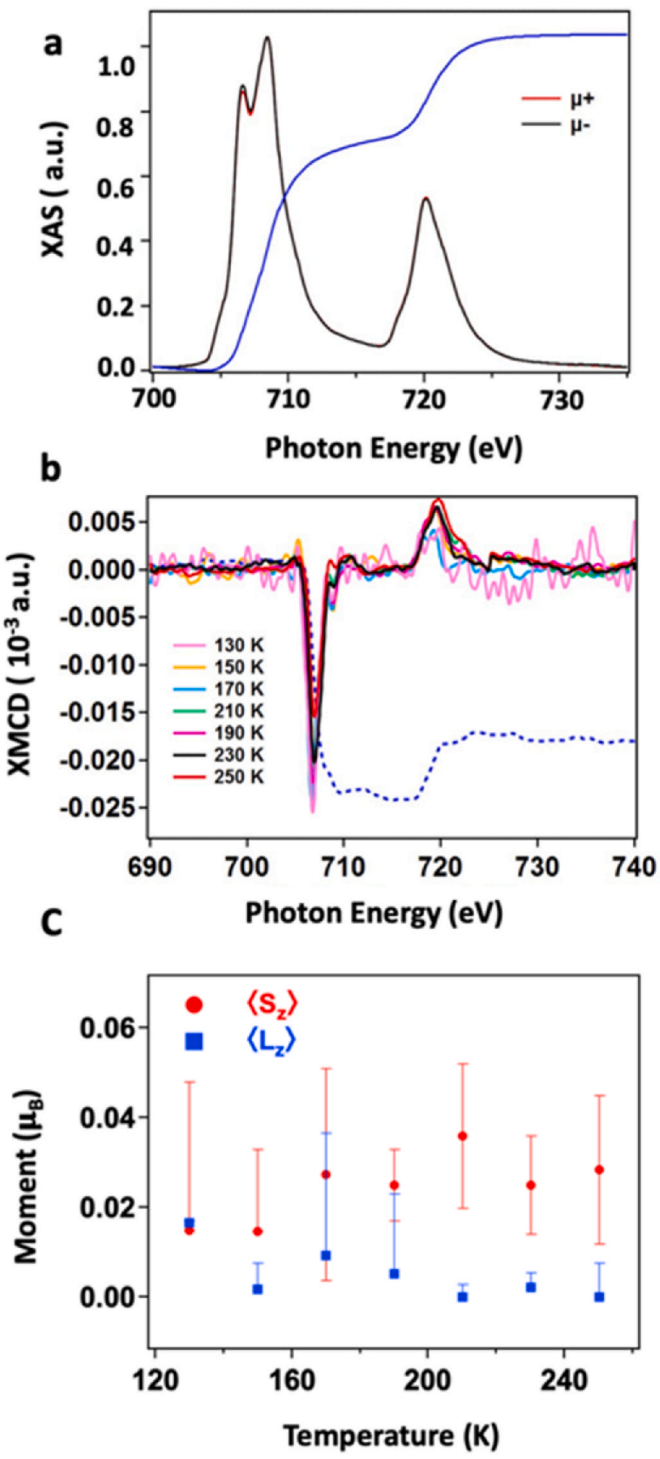

Fig. 2. (a) X-ray absorption spectra and (b) temperature dependent XMCD contrast taken for $[Fe(3\text{-}bpp)_2](TCNQ)_2$ powder near the Fe L edges. (c) Calculated spin and orbital moment with respect to temperature.

spectra in Fig. 1c were taken at temperatures ranging from 50 K to 250 K. The system has a HS state fraction of 0.55 at 50 K which decreases to 0.35 at 60 K, and then increases to above 0.5 as the temperature increases to 250 K. This is distinct from magnetic susceptibility data which show a nearly complete LS state below 100 K and a complete HS state above 120 K (Fig. 1b). Some SCO systems reveal light-induced excited spin-state trapping (LIESST) upon irradiation at low temperatures and return to the LS state with increasing temperature [49–51]. By analogy with the LIESST effect, X-rays can trap the excited spin state at low

temperatures leading to the XIESST effect that is typically suppressed at high temperatures due to rapid relaxation to the ground LS state. The XAS spectra (Fig. 1c) show a similar effect. The modest variation of HS fractions at different temperatures (Fig. 1d) is consistent with the negligible change in the HS fraction found by Üngör et al. [23] using an average Fe–N bond length determined by XRD. The fluence of X-ray from XRD and X-ray absorption could enhance the HS state occupancy even below the thermal spin state transition temperature.

The data presented in Fig. 1d raise the question as to why the fraction of the HS state does not reach 1.0 above 120 K, as expected from the magnetic measurements [18,23,31]. Although this could indicate some damage of the sample through, e.g., by long-term X-ray exposure, our samples appear to be very stable, with nearly complete spin transition observed in magnetic measurements even after prolonged storage. Nevertheless, even small crystallites can exhibit surface effects [47,48,52], so that the surface can exhibit a different LS/HS occupancy ratio than the bulk [48,52,53]. XAS taken in the total electron yield mode, as was done here, is quite surface sensitive and thus can provide an indication of spin state that differs substantially from the bulk [47,48,52,53]. Yet the possibility of the surface affecting the electronic structure needs to be recognized [48,52,53], as this can influence the transport properties in the thin film limit.

Chirality effects in molecules arise from mirror symmetry breaking due to large spin-orbital coupling or crystal packing effects. Mirror symmetry could be lost during molecular deposition on the substrate, the off-center location of the TCNQ, or the imperfect octahedral coordination of the Fe(II), inducing chirality effects, as seen with several amino acids on surfaces [54,55]. Chirality effects, for example resulting from a loss of inversion symmetry at the top layer of a crystallite, may lead to less successful X-ray excitation of some $[Fe(3\text{-}bpp)_2](TCNQ)_2$ to the HS state and could result in the observed HS state occupancy that is smaller between 60 K and 110 K, if circularly polarized light is used.

In this scenario, it is likely that circularly polarized light preferentially excites some $[Fe(3\text{-}bpp)_2](TCNQ)_2$ species over the others. This contributes to the incomplete spin state transition observed by XAS. While several reports on soft XIESST underlined the central role of secondary electrons in the excitation process [56,57], secondary electron mediated excitations are not expected to be very sensitive to the helicity of circularly polarized light. Overall, the XMCD results indicate that there is imperfect chirality compensation, regardless of the origin. We acknowledge this chiral effect could be due to the lack of center of symmetry at the surface. Several studies have been done on these chirality effects on the SCO materials [58–60]. As a single layer of the $[Fe(3\text{-}bpp)_2](TCNQ)_2$ co-crystal has no inversion symmetry [23,31], the surface interface ensures that there is spin orbit coupling and chiral properties at the $[Fe(3\text{-}bpp)_2](TCNQ)_2$ to vacuum interface. The $[Fe(3\text{-}bpp)_2](TCNQ)_2$ crystal appears to exhibit incomplete chirality compensation which was observed by XMCD measurements.

The temperature dependent XMCD spectra of $[Fe(3\text{-}bpp)_2](TCNQ)_2$ were recorded in the presence of a magnetic field of 3.6 T/μ_0. The XMCD signal decreases with temperature (Fig. 2b). Fig. 2c shows the spin and orbital moments, calculated using the sum rules [61] and the integrals of the XAS and XMCD signals (Fig. 2a and b). We observe a slight increment in the spin moment as the temperature increases from 130 K to 170 K and a possible decrease in the orbital moment with increasing temperature. The latter trend is due to enhanced molecular dynamic motion. It is generally expected that for a moment paramagnet, the spin moment would decrease with increasing temperature but in this study, we see little evidence of a significant incremental change in the spin moment with temperature. The increased spin moment with increasing temperature is more difficult to understand and further investigation is indicated.

Adding TCNQ to $[Fe\{H_2B(pz)_2\}_2(bipy)]$ or growing $[Fe\{H_2B(pz)_2\}_2(bipy)]$ thin films from solution locks $[Fe\{H_2B(pz)_2\}_2(bipy)]$ largely in the LS state. Fig. 3 shows the Fe 2*p* (*L*-edge) XAS data of $[Fe\{H_2B(pz)_2\}_2(bipy)]$+TCNQ and pure $[Fe\{H_2B(pz)_2\}_2(bipy)]$ thin films.

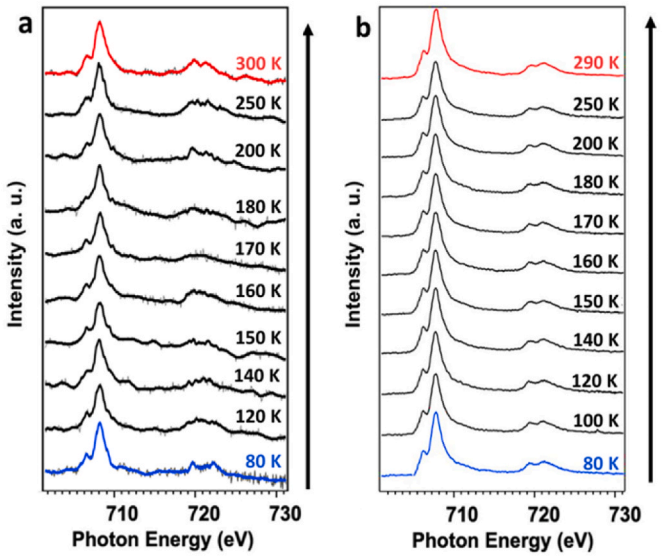

Fig. 3. X-ray absorption spectra with increasing temperature for (a) $[Fe\{H_2B(pz)_2\}_2(bipy)]$+TCNQ (with the filtered data in bold) and (b) pure $[Fe\{H_2B(pz)_2\}_2(bipy)]$ film. In both cases, the spin state remains largely unaffected by the temperature change.

With increasing temperature, both $[Fe\{H_2B(pz)_2\}_2(bipy)]$+TCNQ (Fig. 3a) and $[Fe\{H_2B(pz)_2\}_2(bipy)]$ (Fig. 3b) are mostly locked in the LS state. This indicates that the solvent removal process affects the packing of $[Fe\{H_2B(pz)_2\}_2(bipy)]$ molecules by 'freezing' the thin film largely into the LS state. While it is known that adding polar molecules can lock the spin state [20], the solvent can play an important role too. This is consistent with previous reports that the addition or removal of solvent molecules can alter the nature of the spin transition [62,63].

The challenges associated with the inclusion of interstitial solvent molecules have been highlighted in recent reports on the co-crystallization of SCO cation $[Fe(3\text{-}bpp)_2]^{2+}$ (3-bpp = 2,6-bis(pyrazol-3-yl)pyridine) with the $TCNQ^{\delta-}$ anions [23,31]. Different charges of the $TCNQ^{\delta-}$ ($0 < \delta \leq 1$) and varying interstitial solvent content alter the SCO temperature, thermal hysteresis, and conductivity. Among these materials, $[Fe(3\text{-}bpp)_2](TCNQ)_2 \bullet 3MeCN$ has been shown to undergo complete desolvation without the loss of crystallinity. Moreover, the desolvated complex, $[Fe(3\text{-}bpp)_2](TCNQ)_2$, exhibits an abrupt SCO with the transition temperature of 106 K upon cooling and 117 K upon warming [23]. Comparing XAS of both complexes demonstrates a spin transition for $[Fe(3\text{-}bpp)_2](TCNQ)_2$, even though it is photoactive, and a locked LS state without apparent spin transition for $[Fe\{H_2B(pz)_2\}_2(bipy)]$ combined with TCNQ.

3.1. *Transport properties for composites of $[Fe\{H_2B(pz)_2\}_2(bipy)]$ and TCNQ*

$[Fe(3\text{-}bpp)_2](TCNQ)_2$ shows a room-temperature conductance of 10^{-6} S cm^{-1} [23]. Such low conductivity is due to the dimerization of integer charged $TCNQ^-$ anions [23]. Current and capacitance measurements of $[Fe\{H_2B(pz)_2\}_2(bipy)]$ with the addition of TCNQ are shown in Fig. 4. Mixing TCNQ with $[Fe\{H_2B(pz)_2\}_2(bipy)]$ enhances the conductivity (Fig. 4a) of the LS state compared to the conductivity of pure $[Fe\{H_2B(pz)_2\}_2(bipy)]$ (Fig. S1) and reduces the resistance to about 10^4 Ω cm. For a two terminal diode like device based on pure $[Fe\{H_2B(pz)_2\}_2(bipy)]$ the resistivity can be estimated as about 10^6 Ω cm (off-state, LS state) and about 10^3 Ω cm (on-state, HS state) [10]. As mentioned in the introduction, prospective non-volatile molecular memory devices, based on SCO complexes, requires switching between two spin states at room temperature without either being locked.

Using these current and capacitance measurements, the drift carrier

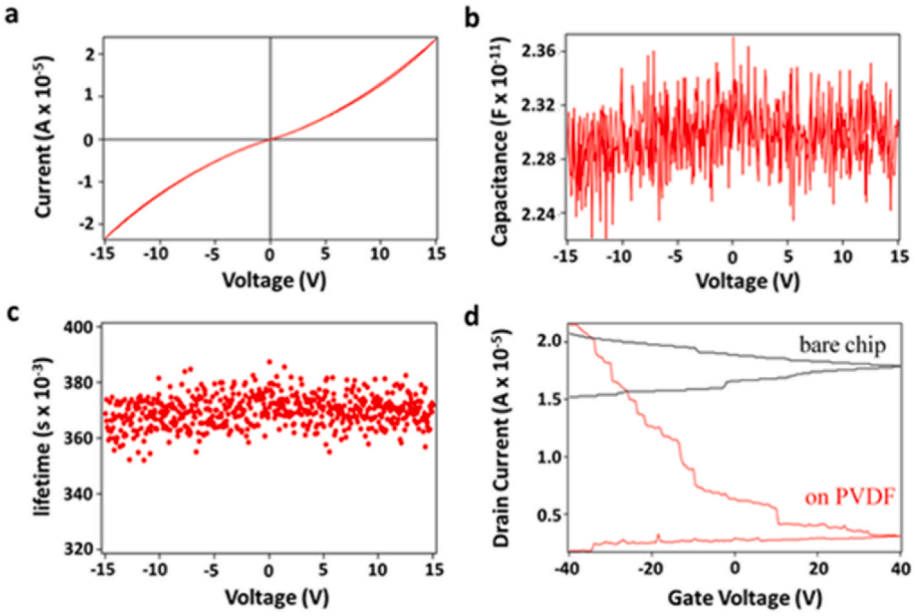

Fig. 4. Electronic transport properties of [Fe{$H_2B(pz)_2$}$_2$(bipy)]+TCNQ composite thin films. (a) Current-voltage and (b) capacitance-voltage curves at room temperature. (c) Drift carrier lifetime and (d) transistor curves, taken at V_{DS} = 15 V for [Fe{$H_2B(pz)_2$}$_2$(bipy)]+TCNQ composite film on bare chip compared to [Fe{$H_2B(pz)_2$}$_2$(bipy)]+TCNQ composite film deposited on ferroelectric PVDF (red). (For interpretation of the references to colour in this figure legend, the reader is referred to the Web version of this article.)

lifetime τ was calculated [64–70].

$$\tau = \frac{\left(\left(\left(\frac{C_D\omega\sqrt{2}}{G_0}\right)^2 + 1\right)^2 - 1\right)^2}{\omega},$$

with the conductance $G_0 = dI/dV$ and the frequency-dependent diffusion capacitance

$$C_D = \frac{G_0}{\omega\sqrt{2}}\left(\sqrt{1+\omega^2\tau^2} - 1\right)^{\frac{1}{2}}.$$

The drift carrier lifetime (Fig. 4c) is in the sub seconds range and indicates a longer recombination time in [Fe{$H_2B(pz)_2$}$_2$(bipy)] with TCNQ as compared to the recombination time of the TCNQ-free complex.

Even though [Fe(3-bpp)$_2$](TCNQ)$_2$ shows a clear spin transition, it has low conductivity at room temperature [23]. However [Fe{$H_2B(pz)_2$}$_2$(bipy)]+TCNQ shows high conductivity at room temperature even though it is locked in the LS state. Even more remarkable is the very long drift carrier lifetimes. Since adding TCNQ enhances the conductivity of [Fe{$H_2B(pz)_2$}$_2$(bipy)] thin films, even though the material is locked in the LS state, it offers the possibility to develop an organic non-volatile memory device.

To explore the potential of [Fe{$H_2B(pz)_2$}$_2$(bipy)] + TCNQ composite thin films for transistor elements, a thin film was deposited on an organic field-effect transistor chip (Fig. 4d). Measurements were taken with a constant drain-source voltage (V_{ds}) of 15 V. The drain current shape indicates charge trapping of holes and electrons and this charge trapping is not equal.

The current versus voltage, I(V), and capacitance versus voltage, C (V), measurements for the [Fe{$H_2B(pz)_2$}$_2$(bipy)] + TCNQ composite thin film were compared to the [Fe{$H_2B(pz)_2$}$_2$(bipy)] + TCNQ composite thin film deposited on PVDF-HFP, a polymer ferroelectric. The conductivity of composite thin film of [Fe{$H_2B(pz)_2$}$_2$(bipy)] plus TCNQ deposited on PVDF-HFP is higher (Fig. S2) compared to the conductivity of the [Fe{$H_2B(pz)_2$}$_2$(bipy)] plus TCNQ composite thin film alone. The PVDF-HFP substrate layer may affect the electron density at the [Fe{H_2B(pz)$_2$}$_2$(bipy)]+TCNQ interface as a result of the strong PVDF electric dipole moments [37,71]. This ferroelectric polymer tends to adopt a preferential polarization direction [72] that could well enhance this redistribution of charge population effect. This interface with this organic ferroelectric does appear to affect the whole [Fe{H_2B(pz)$_2$}$_2$(bipy)]+TCNQ film, as there is a significant enhancement of the conductivity.

The transistor measurements also show that the current for [Fe{H_2B(pz)$_2$}$_2$(bipy)] with TCNQ deposited on PVDF-HFP is higher compared to the [Fe{$H_2B(pz)_2$}$_2$(bipy)] with TCNQ composite thin film alone, although both show similar transistor transfer curves. If we consider the slope of the two curves, deposited on bare chip (black) and PVDF-HFP (red), the slope is higher when the PVDF-HFP dielectric layer is used in the transistor. This indicates that the adjacent layer of PVDF-HFP makes the Fe^{2+} complex more cationic. The drain current decreases with increasing gate voltage from negative to positive voltage suggesting that the hole carrier concentration dominates over the electron carrier concentration.

From the I(V) and C(V) measurements for the [Fe{$H_2B(pz)_2$}$_2$(bipy)] plus TCNQ, the drift carrier lifetime calculated for the [Fe{H_2B(pz)$_2$}$_2$(bipy)] combined with TCNQ composite thin film deposited on PVDF-HFP is also higher compared to the [Fe{$H_2B(pz)_2$}$_2$(bipy)] thin TCNQ alone, which is consistent with the enhanced conductivity of [[Fe{$H_2B(pz)_2$}$_2$(bipy)] with TCNQ composite thin film deposited on PVDF-HFP compared to the [Fe{$H_2B(pz)_2$}$_2$(bipy)] plus TCNQ composite thin film alone.

The carrier mobility was calculated for [Fe{$H_2B(pz)_2$}$_2$(bipy)] plus TCNQ composite thin film alone and deposited on PVDF-HFP using [73–75].

$$\mu_{eff} = \frac{\partial I_d}{\partial V_G}\frac{L}{W}\frac{1}{V_d C_i}$$

where L and W are channel length and width, respectively, C_i is the gate dielectric capacitance per unit area, and V_d is the drain potential. The effective carrier mobility is calculated using the gradient of the transistor curve ($\partial I_d/\partial V_G$) of both [Fe{$H_2B(pz)_2$}$_2$(bipy)] combined with TCNQ on the bare chip with an oxide dielectric and on PVDF is 5×10^{-5} $cm^2\ V^{-1}\ s^{-1}$ and 50×10^{-5} $cm^2\ V^{-1}\ s^{-1}$. This is low mobility but is higher than the mobility values generally expected for organic electronics and corroborates the scenario of charge trapping and coincides with the higher lifetime obtained for the mixtures on bare chip and on PVDF.

We can generalize the appearance of enhanced conductivity as a result of the PVDF-HFP substrate. Not only does [Fe{$H_2B(pz)_2$}$_2$(bipy)] + TCNQ system exhibit enhanced conductivity on the PVDF derivative, but [Fe{$H_2B(pz)_2$}$_2$(bipy)] films by themselves (without TCNQ) exhibit

enhanced conductivity when deposited on PVDF-HFP (supplementary materials Fig. S3). In fact, this effect of the PVDF-HFP substrate extends to the Fe(III) system [Fe(qsal)$_2$[TCNQ$_2$]. Although [Fe(qsal)$_2$[TCNQ$_2$] neither exhibits spin crossover, nor is this molecule an Fe(II) complex (it is Fe(III)) it does show an increment in conductance when deposited on PVDF-HFP (supplementary materials Fig. S4). We note that Fe(III) systems can also show enhance conductivity when combined with TCNQ [29].

4. Conclusion

In conclusion, the [Fe(3-bpp)$_2$](TCNQ)$_2$ co-crystal exhibits a LIEEST like effect during X-ray absorption yet retains a small but clear spin transition with temperature. As measured with XAS, there is an incomplete occupancy of either the LS state or HS state due to photoactivity. The [Fe(3-bpp)$_2$](TCNQ)$_2$ crystal appears to exhibit large surface effects, as have been seen before with SCO polymers [48,52], that could influence conductivity in the thin film limit. [Fe{H$_2$B(pz)$_2$}$_2$(bipy)] mixed with TCNQ is locked in the LS state like pure [Fe{H$_2$B(pz)$_2$}$_2$(bipy)] and this may be due to the solvent used to prepare the thin film. The conductivity of [Fe{H$_2$B(pz)$_2$}$_2$(bipy)] thin films increases with the addition of TCNQ polar molecules despite being locked in the LS state but remains lower than what was previously reported for [Fe(3-bpp)$_2$](TCNQ)$_2$ co-crystals. It is clear that conductivity is enhanced by adding TCNQ polar molecules. The materials challenge here is that the fabrication of molecular SCO systems, when combined with TCNQ, requires preservation of the spin state change and associated conductance for reliable organic thin film devices. This suggests that while the addition of TCNQ to molecular SCO systems is promising, as seen here, the compilations, affecting the spin state transition, resulting from the choice of solvent [62,63] and dipolar molecular additions [19,20] need to be better understood and addressed as this is important when developing a device. In spite of these challenges, this work provides one of the few examples (along with [22]) where the majority carrier of a SCO complex, with an additive like TCNQ, has definitely been determined to be holes through the fabrication of a transistor. The hole doping of the SCO complex, by TCNQ, is not unexpected [18,31].

CRediT authorship contribution statement

Thilini K. Ekanayaka: Conceptualization, Data curation, Formal analysis, Investigation, Methodology, Project administration, Software, Validation, Visualization, Writing – original draft. **Ökten Üngör:** Data curation, Formal analysis, Investigation. **Yuchen Hu:** Data curation. **Esha Mishra:** Data curation, Investigation. **Jared P. Phillips:** Data curation, Investigation. **Ashley S. Dale:** Data curation, Investigation. **Saeed Yazdani:** Data curation, Investigation. **Ping Wang:** Data curation. **Kayleigh A. McElveen:** Data curation. **M. Zaid Zaz:** Data curation. **Jian Zhang:** Resources. **Alpha T. N'Diaye:** Data curation, Investigation, Resources. **Christoph Klewe:** Investigation. **Padraic Shafer:** Formal analysis, Funding acquisition, Resources, Software. **Rebecca Y. Lai:** Resources. **Robert Streubel:** Data curation, Formal analysis, Funding acquisition, Investigation, Resources, Software, Writing – original draft, Writing – review & editing. **Ruihua Cheng:** Funding acquisition, Resources. **Michael Shatruk:** Conceptualization, Formal analysis, Funding acquisition, Methodology, Project administration, Resources, Supervision, Validation, Visualization, Writing – review & editing. **Peter A. Dowben:** Conceptualization, Formal analysis, Funding acquisition, Methodology, Project administration, Resources, Supervision, Software, Validation, Visualization, Writing – original draft, Writing – review & editing.

Declaration of competing interest

The authors declare that they have no known competing financial interests or personal relationships that could have appeared to influence the work reported in this paper.

Data availability

Data will be made available on request.

Acknowledgements

This research was supported by the National Science Foundation through NSF-DMR 2003057 [T. Ekanayaka, E. Mishra, J. P. Phillips, R. Cheng, Md. Z. Zaz, P. A. Dowben], the EPSCoR RII Track-1: Emergent Quantum Materials and Technologies (EQUATE), Award OIA-2044049 [K. A. McElveen, R. Y. Lai and R. Streubel] and a Nebraska EPSCoR FIRST Award #OIA-1557417 [R. Streubel]. Use of the Advanced Light Source, Lawrence Berkeley National Laboratory, was supported by the U.S. Department of Energy (DOE) under contract no. DE-AC02-05CH11231. The synthesis and magnetic characterization of the complex was carried out by the Shatruk group as part of research on the NSF grant CHE-1955754.

Appendix A. Supplementary data

Supplementary data to this article can be found online at https://doi.org/10.1016/j.matchemphys.2022.127276.

References

[1] B. Capozzi, J. Xia, O. Adak, E.J. Dell, Z.-F. Liu, J.C. Taylor, J.B. Neaton, L. M. Campos, L. Venkataraman, Single-molecule diodes with high rectification ratios through environmental control, Nat. Nanotechnol. 10 (2015) 522–527, https://doi.org/10.1038/nnano.2015.97.
[2] M. Elbing, R. Ochs, M. Koentopp, M. Fischer, C. von Hanisch, F. Weigend, F. Evers, H.B. Weber, M. Mayor, A single-molecule diode, Proc. Natl. Acad. Sci. USA 102 (2005) 8815–8820, https://doi.org/10.1073/pnas.0408888102.
[3] M.L. Perrin, M. Doelman, R. Eelkema, H.S.J. van der Zant, Design of an efficient coherent multi-site single-molecule rectifier, Phys. Chem. Chem. Phys. 19 (2017) 29187–29194, https://doi.org/10.1039/C7CP04456A.
[4] X. Chen, M. Roemer, L. Yuan, W. Du, D. Thompson, E. del Barco, C.A. Nijhuis, Molecular diodes with rectification ratios exceeding 105 driven by electrostatic interactions, Nat. Nanotechnol. 12 (2017) 797–803, https://doi.org/10.1038/nnano.2017.110.
[5] X. Guo, Single-molecule electrical biosensors based on single-walled carbon nanotubes, Adv. Mater. 25 (2013) 3397–3408, https://doi.org/10.1002/adma.201301219.
[6] Z. Li, M. Smeu, S. Afsari, Y. Xing, M.A. Ratner, E. Borguet, Single-molecule sensing of environmental pH-an STM break junction and NEGF-DFT approach, Angew. Chem. 53 (2014) 1098–1102, https://doi.org/10.1002/anie.201308398.
[7] S. Kubatkin, A. Danilov, M. Hjort, J. Cornil, J.-L. Brédas, N. Stuhr-Hansen, P. Hedegård, T. Bjørnholm, Single-electron transistor of a single organic molecule with access to several redox states, Nature 425 (2003) 698–701, https://doi.org/10.1038/nature02010.
[8] N. Xin, X. Li, C. Jia, Y. Gong, M. Li, S. Wang, G. Zhang, J. Yang, X. Guo, Tuning charge transport in aromatic-ring single-molecule junctions via ionic-liquid gating, Angew. Chem. 130 (2018) 14222–14227, https://doi.org/10.1002/ange.201807465.
[9] G. Hao, R. Cheng, P.A. Dowben, The emergence of the local moment molecular spin transistor, J. Phys. Condens. Matter 32 (2020), 234002, https://doi.org/10.1088/1361-648X/ab74e4.
[10] T.K. Ekanayaka, G. Hao, A. Mosey, A.S. Dale, X. Jiang, A.J. Yost, K.R. Sapkota, G. T. Wang, J. Zhang, A.T. N'Diaye, A. Marshall, R. Cheng, A. Naeemi, X. Xu, P. A. Dowben, Nonvolatile voltage controlled molecular spin-state switching for memory applications, Magnetochemistry 7 (2021) 37, https://doi.org/10.3390/magnetochemistry7030037.
[11] P. Gütlich, Y. Garcia, H.A. Goodwin, Spin crossover phenomena in Fe(ii) complexes, Chem. Soc. Rev. 29 (2000) 419–427, https://doi.org/10.1039/b003504l.
[12] W. Nicolazzi, A. Bousseksou, Thermodynamical aspects of the spin crossover phenomenon, C. R. Chim. 21 (2018) 1060–1074, https://doi.org/10.1016/j.crci.2018.10.003.
[13] P. Gütlich, A.B. Gaspar, Y. Garcia, Spin state switching in iron coordination compounds, Beilstein J. Org. Chem. 9 (2013) 342–391, https://doi.org/10.3762/bjoc.9.39.
[14] K. Ridier, G. Molnár, L. Salmon, W. Nicolazzi, A. Bousseksou, Hysteresis, nucleation and growth phenomena in spin-crossover solids, Solid State Sci. 74 (2017) A1–A22, https://doi.org/10.1016/j.solidstatesciences.2017.10.014.

[15] A. Hauser, J. Jeftić, H. Romstedt, R. Hinek, H. Spiering, Cooperative phenomena and light-induced bistability in iron(II) spin-crossover compounds, Coord. Chem. Rev. 190–192 (1999) 471–491, https://doi.org/10.1016/S0010-8545(99)00111-3.

[16] G. Hao, A. Mosey, X. Jiang, A.J. Yost, K.R. Sapkota, G.T. Wang, X. Zhang, J. Zhang, A.T. N'Diaye, R. Cheng, X. Xu, P.A. Dowben, Nonvolatile voltage controlled molecular spin state switching, Appl. Phys. Lett. 114 (2019), 032901, https://doi.org/10.1063/1.5054909.

[17] A. Mosey, A.S. Dale, G. Hao, A. N'Diaye, P.A. Dowben, R. Cheng, Quantitative study of the energy changes in voltage-controlled spin crossover molecular thin films, J. Phys. Chem. Lett. 11 (2020) 8231–8237, https://doi.org/10.1021/acs.jpclett.0c02209.

[18] H. Phan, S.M. Benjamin, E. Steven, J.S. Brooks, M. Shatruk, Photomagnetic response in highly conductive iron(II) spin-crossover complexes with TCNQ radicals, Angew. Chem. 127 (2015) 837–841, https://doi.org/10.1002/ange.201408680.

[19] P. Costa, G. Hao, A.T. N'Diaye, L. Routaboul, P. Braunstein, X. Zhang, J. Zhang, B. Doudin, A. Enders, P.A. Dowben, Perturbing the spin crossover transition activation energies in Fe(H $_2$ B(pz)$_2$)$_2$(bipy) with zwitterionic additions, J. Phys. Condens. Matter 30 (2018), 305503, https://doi.org/10.1088/1361-648X/aacd7e.

[20] P.S. Costa, G. Hao, A.T. N'Diaye, L. Routaboul, P. Braunstein, X. Zhang, J. Zhang, T.K. Ekanayaka, Q.-Y. Shi, V. Schlegel, B. Doudin, A. Enders, P.A. Dowben, Manipulation of the molecular spin crossover transition of Fe(H$_2$B(pz)$_2$)$_2$(bipy) by addition of polar molecules, J. Phys. Condens. Matter 32 (2020), 034001, https://doi.org/10.1088/1361-648X/ab468c.

[21] D. Nieto-Castro, F.A. Garcés-Pineda, A. Moneo-Corcuera, I. Sánchez-Molina, J. R. Galán-Mascarós, Mechanochemical processing of highly conducting organic/inorganic composites exhibiting spin crossover–induced memory effect in their transport properties, Adv. Funct. Mater. 31 (2021), 2102469, https://doi.org/10.1002/adfm.202102469.

[22] E. Mishra, T.K. Ekanayaka, K.A. McElveen, R.Y. Lai, P.A. Dowben, Evidence for long drift carrier lifetimes in [Fe(Htrz)$_2$(trz)](BF$_4$) plus polyaniline composites, Org. Electron. (2022), 106516, https://doi.org/10.1016/j.orgel.2022.106516.

[23] Ö. Üngör, E.S. Choi, M. Shatruk, Optimization of crystal packing in semiconducting spin-crossover materials with fractionally charged TCNQ$^{\delta\,-}$ anions ($0 < \delta < 1$), Chem. Sci. 12 (2021) 10765–10779, https://doi.org/10.1039/D1SC02843J.

[24] Y.N. Shvachko, D.V. Starichenko, A.V. Korolyov, E.B. Yagubskii, A.I. Kotov, L. I. Buravov, K.A. Lyssenko, V.N. Zverev, S.V. Simonov, L.V. Zorina, O.G. Shakirova, L.G. Lavrenova, The conducting spin-crossover compound combining Fe(II) cation complex with TCNQ in a fractional reduction state, Inorg. Chem. 55 (2016) 9121–9130, https://doi.org/10.1021/acs.inorgchem.6b01829.

[25] V. Rubio-Giménez, S. Tatay, C. Martí-Gastaldo, Electrical conductivity and magnetic bistability in metal–organic frameworks and coordination polymers: charge transport and spin crossover at the nanoscale, Chem. Soc. Rev. 49 (2020) 5601–5638, https://doi.org/10.1039/C9CS00594C.

[26] M. Wang, Z.-Y. Li, R. Ishikawa, M. Yamashita, Spin crossover and valence tautomerism conductors, Coord. Chem. Rev. 435 (2021), 213819, https://doi.org/10.1016/j.ccr.2021.213819.

[27] R. Ishikawa, S. Ueno, S. Nifuku, Y. Horii, H. Iguchi, Y. Miyazaki, M. Nakano, S. Hayami, S. Kumagai, K. Katoh, Z. Li, M. Yamashita, S. Kawata, Simultaneous spin-crossover transition and conductivity switching in a dinuclear iron(II) coordination compound based on 7,7′,8,8′-tetracyano- *p* -quinodimethane, Chem. Eur J. 26 (2020) 1278–1285, https://doi.org/10.1002/chem.201903934.

[28] A.V. Kazakova, A.V. Tiunova, D.V. Korchagin, G.V. Shilov, E.B. Yagubskii, V. N. Zverev, S.C. Yang, J. Lin, J. Lee, O.V. Maximova, A.N. Vasiliev, The first conducting spin-crossover compound combining a Mn ^{III} cation complex with electroactive TCNQ demonstrating an abrupt spin transition with a hysteresis of 50 K, Chem. Eur J. 25 (2019) 10204–10213, https://doi.org/10.1002/chem.201901792.

[29] Y.N. Shvachko, D.V. Starichenko, A.V. Korolyov, A.I. Kotov, L.I. Buravov, V. N. Zverev, S.V. Simonov, L.V. Zorina, E.B. Yagubskii, The highly conducting spin-crossover compound combining Fe(III) cation complex with TCNQ in a fractional reduction state. Synthesis, structure, electric and magnetic properties, Magnetochemistry 3 (2017) 9, https://doi.org/10.3390/magnetochemistry3010009.

[30] Y.N. Shvachko, D.V. Starichenko, A.V. Korolyov, E.B. Yagubskii, A.I. Kotov, L. I. Buravov, K.A. Lyssenko, V.N. Zverev, S.V. Simonov, L.V. Zorina, O.G. Shakirova, L.G. Lavrenovag, The conducting spin-crossover compound combining Fe(II) cation complex with TCNQ in a fractional reduction state, Inorg. Chem. 55 (2016) 9121–9130, https://doi.org/10.1021/acs.inorgchem.6b01829.

[31] N. Schmidt, M. Stöhr, Molecular self-assembly on graphene: the role of the substrate, in: Encyclopedia of Interfacial Chemistry, Elsevier, 2018, pp. 110–119, https://doi.org/10.1016/B978-0-12-409547-2.14162-9.

[32] Ö. Üngör, E.S. Choi, M. Shatruk, Solvent-dependent spin-crossover behavior in semiconducting Co–crystals of [Fe(1-bpp)$_2$]$^{2+}$ cations and TCNQ $^{\delta-}$ anions (0<δ<1), 2021, Eur. J. Inorg. Chem. (2021) 4812–4820, https://doi.org/10.1002/ejic.202100707.

[33] T. Palamarciuc, J.C. Oberg, F. El Hallak, C.F. Hirjibehedin, M. Serri, S. Heutz, J.-F. Létard, P. Rosa, Spin crossover materials evaporated under clean high vacuum and ultra-high vacuum conditions: from thin films to single molecules, J. Mater. Chem. 22 (2012) 9690, https://doi.org/10.1039/c2jm15094h.

[34] L.R. Melby, R.J. Harder, W.R. Hertler, W. Mahler, R.E. Benson, W.E. Mochel, Substituted quinodimethans. II. Anion-Radical derivatives and complexes of 7,7,8,8-tetracyanoquinodimethan, J. Am. Chem. Soc. 84 (1962) 3374–3387, https://doi.org/10.1021/ja00876a029.

[35] J. Lee, H. Lee, C. Kiguye, C. Bae, J. Kim, Controllable coating and reshaping of gold nanorods with tetracyanoquinodimethane, Chem. Commun. 55 (2019), 11731, https://doi.org/10.1039/C9CC05603C.

[36] R.C. Dickinson, W.A. Baker Jr., R.L. Collins, The magnetic properties of bis[N-(8-quinolyl)-salicylaldimine]halogenoiron(III)·X hydrate, Fe(8-QS)2X·χH2O: a reexamination, J. Inorg. Nucl. Chem. 39 (1977) 1531–1533, https://doi.org/10.1016/0022-1902(77)80094-8.

[37] S. Ducharme, T.J. Reece, C.M. Othon, R.K. Rannow, Ferroelectric polymer Langmuir-Blodgett films for nonvolatile memory applications, IEEE Trans. Device Mater. Reliab. 5 (2005) 720–735, https://doi.org/10.1109/TDMR.2005.860818.

[38] P. Gütlich, H.A. Goodwin (Eds.), Spin Crossover in Transition Metal Compounds I-III, Springer, Berlin ; New York, 2004.

[39] A. Hauser, Ligand field theoretical considerations, in: P. Gütlich, H.A. Goodwin (Eds.), Spin Crossover in Transition Metal Compounds I, Springer Berlin Heidelberg, Berlin, Heidelberg, 2004, pp. 49–58, https://doi.org/10.1007/b13528.

[40] M. Bernien, H. Naggert, L.M. Arruda, L. Kipgen, F. Nickel, J. Miguel, C. F. Hermanns, A. Krüger, D. Krüger, E. Schierle, E. Weschke, F. Tuczek, W. Kuch, Highly efficient thermal and light-induced spin-state switching of an Fe(II) complex in direct contact with a solid surface, ACS Nano 9 (2015) 8960–8966, https://doi.org/10.1021/acsnano.5b02840.

[41] M. Bernien, D. Wiedemann, C.F. Hermanns, A. Krüger, D. Rolf, W. Kroener, P. Müller, A. Grohmann, W. Kuch, Spin crossover in a vacuum-deposited submonolayer of a molecular iron(II) complex, J. Phys. Chem. Lett. 3 (2012) 3431–3434, https://doi.org/10.1021/jz3011805.

[42] D. Collison, C.D. Garner, C.M. McGrath, J.F.W. Mosselmans, M.D. Roper, J.M. W. Seddon, E. Sinn, N.A. Young, Soft X-ray induced excited spin state trapping and soft X-ray photochemistry at the iron L2,3 edge in [Fe(phen)$_2$(NCS)$_2$] and [Fe(phen)$_2$(NCSe)$_2$] (phen = 1,10-phenanthroline), J. Chem. Soc., Dalton Trans. (1997) 4371–4376, https://doi.org/10.1039/a703728g.

[43] V. Briois, ChC. dit Moulin, Ph Sainctavit, Ch Brouder, A.-M. Flank, Full multiple scattering and crystal field multiplet calculations performed on the spin transition FeII(phen)$_2$(NCS)$_2$ complex at the iron K and L2,3 X-ray absorption edges, J. Am. Chem. Soc. 117 (1995) 1019–1026, https://doi.org/10.1021/ja00108a018.

[44] M. Gruber, T. Miyamachi, V. Davesne, M. Bowen, S. Boukari, W. Wulfhekel, M. Alouani, E. Beaurepaire, Spin crossover in Fe(phen)$_2$(NCS)$_2$ complexes on metallic surfaces, J. Chem. Phys. 146 (2017), 092312, https://doi.org/10.1063/1.4973511.

[45] T. Miyamachi, M. Gruber, V. Davesne, M. Bowen, S. Boukari, L. Joly, F. Scheurer, G. Rogez, T.K. Yamada, P. Ohresser, E. Beaurepaire, W. Wulfhekel, Robust spin crossover and memristance across a single molecule, Nat. Commun. 3 (2012) 938, https://doi.org/10.1038/ncomms1940.

[46] X. Zhang, P.S. Costa, J. Hooper, D.P. Miller, A.T. N'Diaye, S. Beniwal, X. Jiang, Y. Yin, P. Rosa, L. Routaboul, M. Gonidec, L. Poggini, P. Braunstein, B. Doudin, X. Xu, A. Enders, E. Zurek, P.A. Dowben, Locking and unlocking the molecular spin crossover transition, Adv. Mater. 29 (2017), 1702257, https://doi.org/10.1002/adma.201702257.

[47] X. Zhang, S. Mu, G. Chastanet, N. Daro, T. Palamarciuc, P. Rosa, J.-F. Létard, J. Liu, G.E. Sterbinsky, D.A. Arena, C. Etrillard, B. Kundys, B. Doudin, P.A. Dowben, Complexities in the molecular spin crossover transition, J. Phys. Chem. C 119 (2015) 16293–16302, https://doi.org/10.1021/acs.jpcc.5b02220.

[48] T.K. Ekanayaka, H. Kurz, A.S. Dale, G. Hao, A. Mosey, E. Mishra, A.T. N'Diaye, R. Cheng, B. Weber, P.A. Dowben, Probing the unpaired Fe spins across the spin crossover of a coordination polymer, Mater. Adv. 2 (2021) 760–768, https://doi.org/10.1039/D0MA00612B.

[49] B. Rösner, M. Milek, A. Witt, B. Gobaut, P. Torelli, R.H. Fink, M.M. Khusniyarov, Reversible photoswitching of a spin-crossover molecular complex in the solid state at room temperature, Angew. Chem. 127 (2015) 13168–13172, https://doi.org/10.1002/ange.201504192.

[50] J.-J. Lee, H. Sheu, C.-R. Lee, J.-M. Chen, J.-F. Lee, C.-C. Wang, C.-H. Huang, Y. Wang, X-Ray absorption spectroscopic studies on light-induced excited spin state trapping of an Fe(II) complex, J. Am. Chem. Soc. 122 (2000) 5742–5747, https://doi.org/10.1021/ja9943290.

[51] N. Moliner, L. Salmon, L. Capes, M.C. Muñoz, J.-F. Létard, A. Bousseksou, J.-P. Tuchagues, J.J. McGarvey, A.C. Dennis, M. Castro, R. Burriel, J.A. Real, Thermal and optical switching of molecular spin states in the {[FeL[H$_2$B(pz)$_2$]$_2$} spin-crossover system (L = bpy, phen), J. Phys. Chem. B 106 (2002) 4276–4283, https://doi.org/10.1021/jp013872b.

[52] T.K. Ekanayaka, H. Kurz, K.A. McElveen, G. Hao, E. Mishra, A.T. N'Diaye, R.Y. Lai, B. Weber, P.A. Dowben, Evidence for surface effects on the intermolecular interactions in Fe(ii) spin crossover coordination polymers, Phys. Chem. Chem. Phys. 24 (2022) 883–894, https://doi.org/10.1039/D1CP04243B.

[53] X. Jiang, G. Hao, X. Wang, A. Mosey, X. Zhang, L. Yu, A.J. Yost, X. Zhang, A. D. DiChiara, A.T. N'Diaye, X. Cheng, J. Zhang, R. Cheng, X. Xu, P.A. Dowben, Tunable spin-state bistability in a spin crossover molecular complex, J. Phys. Condens. Matter 31 (2019), 315401, https://doi.org/10.1088/1361-648X/ab1a7d.

[54] A. Kühnle, T.R. Linderoth, B. Hammer, F. Besenbacher, Chiral recognition in dimerization of adsorbed cysteine observed by scanning tunnelling microscopy, Nature 415 (2002) 891–893, https://doi.org/10.1038/415891a.

[55] A. Kühnle, T.R. Linderoth, F. Besenbacher, Chiral symmetry breaking observed for cysteine on the Au(110)-(1×2) surface, Top. Catal. 54 (2011) 1384–1391, https://doi.org/10.1007/s11244-011-9765-z.

[56] C. Wäckerlin, F. Donati, A. Singha, R. Baltic, S. Decurtins, S.-X. Liu, S. Rusponi, J. Dreiser, Excited spin-state trapping in spin crossover complexes on ferroelectric substrates, J. Phys. Chem. C 122 (2018) 8202–8208, https://doi.org/10.1021/acs.jpcc.7b10941.

[57] L. Kipgen, M. Bernien, F. Nickel, H. Naggert, A.J. Britton, L.M. Arruda, E. Schierle, E. Weschke, F. Tuczek, W. Kuch, Soft-x-ray-induced spin-state switching of an adsorbed Fe(II) spin-crossover complex, J. Phys. Condens. Matter 29 (2017), 394003, https://doi.org/10.1088/1361-648X/aa7e52.

[58] T.K. Ekanayaka, P. Wang, S. Yazdani, J.P. Phillips, E. Mishra, A.S. Dale, A. T. N'Diaye, C. Klewe, P. Shafer, J. Freeland, R. Streubel, J.P. Wampler, V. Zapf, R. Cheng, M. Shatruk, P.A. Dowben, Evidence of dynamical effects and critical field in a cobalt spin crossover complex, 10.1039.D1CC05309D, Chem. Commun. (2022), https://doi.org/10.1039/D1CC05309D.

[59] W. Liu, X. Bao, L.-L. Mao, J. Tucek, R. Zboril, J.-L. Liu, F.-S. Guo, Z.-P. Ni, M.-L. Tong, A chiral spin crossover metal–organic framework, Chem. Commun. 50 (2014) 4059–4061, https://doi.org/10.1039/C3CC48935C.

[60] L.-F. Qin, C.-Y. Pang, W.-K. Han, F.-L. Zhang, L. Tian, Z.-G. Gu, X. Ren, Z. Li, Spin crossover properties of enantiomers, co-enantiomers, racemates, and co-racemates, Dalton Trans. 45 (2016) 7340–7348, https://doi.org/10.1039/C6DT00210B.

[61] C.T. Chen, Y.U. Idzerda, H.-J. Lin, N.V. Smith, G. Meigs, E. Chaban, G.H. Ho, E. Pellegrin, F. Sette, Experimental confirmation of the X-ray magnetic circular dichroism sum rules for iron and cobalt, Phys. Rev. Lett. 75 (1995) 152–155, https://doi.org/10.1103/PhysRevLett.75.152.

[62] A.-C. Bas, V. Shalabaeva, X. Thompson, L. Vendier, L. Salmon, C. Thibault, G. Molnár, L. Routaboul, A. Bousseksou, Effects of solvent vapor annealing on the crystallinity and spin crossover properties of thin films of $[Fe(HB(tz)_3)_2]$, C. R. Chim. 22 (2019) 525–533, https://doi.org/10.1016/j.crci.2019.03.002.

[63] S. Rat, K. Ridier, L. Vendier, G. Molnár, L. Salmon, A. Bousseksou, Solvatomorphism and structural-spin crossover property relationship in bis [hydrotris(1,2,4-triazol-1-yl)borate]iron(ii), CrystEngComm 19 (2017) 3271–3280, https://doi.org/10.1039/C7CE00741H.

[64] C.C. Ilie, F. Guzman, B.L. Swanson, I.R. Evans, P.S. Costa, J.D. Teeter, M. Shekhirev, N. Benker, S. Sikich, A. Enders, P.A. Dowben, A. Sinitskii, A.J. Yost, Inkjet printable-photoactive all inorganic perovskite films with long effective photocarrier lifetimes, J. Phys. Condens. Matter 30 (2018) 18LT02, https://doi.org/10.1088/1361-648X/aab986.

[65] G.G. Peterson, E. Echeverria, B. Dong, J.P. Silva, E.R. Wilson, J.A. Kelber, M. Nastasi, P.A. Dowben, Increased drift carrier lifetime in semiconducting boron carbides deposited by plasma enhanced chemical vapor deposition from carboranes and benzene, J. Vac. Sci. Technol.: Vacuum, Surfaces, and Films 35 (2017), 03E101, https://doi.org/10.1116/1.4973338.

[66] A. Oyelade, A.J. Yost, N. Benker, B. Dong, S. Knight, M. Schubert, P.A. Dowben, J. A. Kelber, Composition-dependent charge transport in boron carbides alloyed with aromatics: plasma enhanced chemical vapor deposition aniline/orthocarborane films, Langmuir 34 (2018) 12007–12016, https://doi.org/10.1021/acs.langmuir.8b02114.

[67] G.G. Peterson, Q. Su, Y. Wang, N.J. Ianno, P.A. Dowben, M. Nastasi, Improved α-$B_{10}C_{2+x}H_y$/Si p-n heterojunction performance after neutron irradiation, Journal of Vacuum Science & Technology B, Nanotechnology and Microelectronics: Materials, Processing, Measurement, and Phenomena 36 (2018), 011207, https://doi.org/10.1116/1.5008999.

[68] A. Oyelade, A. Osonkie, A.J. Yost, N. Benker, P.A. Dowben, J.A. Kelber, Optical, electronic and visible-range photo-electronic properties of boron carbide-indole films, J. Phys. D Appl. Phys. 53 (2020), 355101, https://doi.org/10.1088/1361-6463/ab8e7e.

[69] E. Echeverria, B. Dong, G. Peterson, J.P. Silva, E.R. Wilson, M.S. Driver, Y.-S. Jun, G.D. Stucky, S. Knight, T. Hofmann, Z.-K. Han, N. Shao, Y. Gao, W.-N. Mei, M. Nastasi, P.A. Dowben, J.A. Kelber, Semiconducting boron carbides with better charge extraction through the addition of pyridine moieties, J. Phys. D Appl. Phys. 49 (2016), 355302, https://doi.org/10.1088/0022-3727/49/35/355302.

[70] Z.G. Marzouk, A. Dhingra, Y. Burak, V. Adamiv, I. Teslyuk, P.A. Dowben, Long carrier lifetimes in crystalline lithium tetraborate, Mater. Lett. 297 (2021), 129978, https://doi.org/10.1016/j.matlet.2021.129978.

[71] L.M. Blinov, V.M. Fridkin, S.P. Palto, A.V. Bune, P.A. Dowben, S. Ducharme, Two-Dimensional Ferroelectrics, Russian edition, vol. 170, *Uspekhi Fizicheskikh Nauk*, 2000, pp. 247–262, https://doi.org/10.1070/PU2000v043n03ABEH000639. *Ph*ysics Uspekhi [English edition volume] 43 (2000) 243-257.

[72] Chun-gang Duan, W.N. Mei, Wei-Guo Yin, J. Liu, J.R. Hardy, S. Ducharme, P. A. Dowben, Simulations of ferroelectric polymer film polarization: the role of dipole interactions, *Phys. Rev.* B 69 (2004), 235106, https://doi.org/10.1103/PhysRevB.69.235106.

[73] T. Uemura, C. Rolin, T.-H. Ke, P. Fesenko, J. Genoe, P. Heremans, J. Takeya, On the extraction of charge carrier mobility in high-mobility organic transistors, Adv. Mater. 28 (2016) 151–155, https://doi.org/10.1002/adma.201503133.

[74] S.M. Sze, Physics of Semiconductor Devices, vol. 2, Wiley, New York, N.Y., 1981.

[75] C. Tanase, E.J. Meijer, P.W.M. Blom, D.M. de Leeuw, Local charge carrier mobility in disordered organic field-effect transistors, Org. Electron. 4 (2003) 33–37, https://doi.org/10.1016/S1566-1199(03)00006-5.